applied sciences

MDPI

Article

Influence of Stress Anisotropy on Petrophysical Parameters of Deep and Ultradeep Tight Sandstone

Hui Zhang [1], Ke Xu [1,*], Binxin Zhang [2], Guoqing Yin [1], Haiying Wang [1], Zhimin Wang [1], Chao Li [1], Shujun Lai [1] and Ziwei Qian [1]

[1] Research Institute of Exploration and Development, Tarim Oilfield Company, PetroChina, Korla 841000, China
[2] Key Laboratory of Tectonics and Petroleum Resources of Ministry of Education, China University of Geosciences, Wuhan 430074, China
* Correspondence: xukee0505@163.com

Abstract: Rock mechanics parameters control the distribution of in situ stress and natural fractures, which is the key to sweet spot evaluation in reservoir engineering. Combined with the distribution of in situ stress, an experimental scheme of stress on rock physical parameters was designed. The results show that rock sonic velocity is extremely sensitive to water saturation under overburden pressure. At ultrasonic frequencies, when the water saturation increases from 0% to 80%, the P-wave velocity increases first and then decreases. When the water saturation continues to increase to 100%, the P-wave velocity increases. This is due to the effect of water saturation on the shear modulus. Saturation is negatively correlated with shear wave velocity and resistivity. Different minerals have different control effects on the rock P-S wave velocity ratio. Quartz content plays a dominant role, and the two are negatively correlated, followed by feldspar and clay, and the two are positively correlated with the P-S wave ratio. The confining pressure, axial compression, stress ratio and burial depth are positively correlated with the P-S wave and negatively correlated with the P-S wave ratio; in descending order, the influencing factors of stress on the petrophysical parameters are maximum stress ratio > confining pressure > axial pressure.

Keywords: deep and ultradeep; in situ stress; tight sandstone; stress anisotropy; petrophysical parameter

check for updates

Citation: Zhang, H.; Xu, K.; Zhang, B.; Yin, G.; Wang, H.; Wang, Z.; Li, C.; Lai, S.; Qian, Z. Influence of Stress Anisotropy on Petrophysical Parameters of Deep and Ultradeep Tight Sandstone. *Appl. Sci.* **2022**, *12*, 11543. https://doi.org/10.3390/app122211543

Academic Editor: Arcady Dyskin

Received: 24 October 2022
Accepted: 11 November 2022
Published: 14 November 2022

1. Introduction

Deep and ultradeep tight sandstone reservoirs are the main reservoirs contributing to the current oil and gas production capacity in China, and are also the key objects of oil and gas research in China. To improve the understanding of deep and ultradeep tight sandstone reservoirs, it is necessary to explore their physical characteristics. The purpose is to study the specific response of rock physical parameters in reservoirs, indicate the specificity of underground rock structures, and identify their effects on oil and gas exploration. Rock mechanical parameters are the basis for numerical simulations of the stress field, reservoir fracture evaluation, and formation fracturing [1–3]. The study of the relationship model between rock mechanical parameters and in situ stress has practical significance for the accurate evaluation of rock mechanical parameters and in situ stress prediction [4–12].

Complex geological structure, surface erosion, multi-stage fracture activity and other factors will influence the complexity and differentiation of in-situ stress distribution. Especially in the vicinity of complex faults, the magnitude and direction of in-situ stress will change to a certain extent. In addition, frequent tectonic activities will cause local faults to produce intricate joints and fissures, which will have a greater impact on the rock properties of the whole local area, thus increasing the difficulty of geological research. Therefore, it is of great theoretical significance to improve the research of in-situ stress for geological exploration.

Wyllie et al. (1958) conducted experimental tests on Berea sandstone and found that the net stress remained unchanged and the sonic velocity changed little with the confining pressure [13]. As the net stress increased, the sonic velocity increased. Birch (1960) found through experimental studies that the P-wave velocities of igneous and metamorphic rocks increased with increasing confining pressure [14]. Igneous rock enlargement was more pronounced. Han et al. (1986) considered that the increase in clay content was the main factor for the decrease in porosity and P-wave velocity [15]. Eberhart-Phillips et al. (1989) found that the relationship between sonic velocity and effective stress in sandstone changed from a power exponent to a linear exponent [9]. Tutuncu et al. (1994) believed that due to the close contact between tight sandstone grains, a large number of microcracks with a small aspect ratio were formed, resulting in the sensitivity of P-wave velocity and S-wave velocity to pressure changes in tight sandstone compared with ordinary sandstone [16]. Ma et al. (2006) found through experiments that the P-wave and the effective stress have an exponential relationship, the velocity and the effective stress have nonlinear change characteristics when the pressure is low, and the velocity changes tend to be stable when the pressure is high [17]. Sandstone saturated with water and oil has no effect on the change in shear wave velocity, but the shear wave velocity when saturated with gas is small. Lithology affects the variation in sonic wave velocity with shear wave velocity. Sandstone is stronger than shale. Through relevant experiments on volcanic rocks, Xiao et al. (2010) found that effective stress and water saturation affected the velocity of the S-wave [18]. When the effective stress is constant, the sonic wave velocity of fully saturated water is large, the sonic wave velocity of bound water saturation is moderate, and the sonic wave velocity of dry rock is small. The variation in the sonic velocity of the rock sample is not controlled by the linear effective stress but increases with a nonlinear increase in the effective stress.

Wang et al. (2014) studied the stress sensitivity of fractured reservoirs in the Keshen gas field by using the reservoir fracture numerical simulation method [19]. The results show that with increasing effective stress, both the porosity and permeability of the fracture decreased, showing strong stress sensitivity, and the stress sensitivity of fracture permeability was stronger than that of fracture porosity. The higher the initial values of the reservoir fracture porosity and permeability parameters are, the stronger the stress sensitivity. For a low-permeability fractured reservoir, the stronger the rock plasticity is, the stronger the stress sensitivity. The effective stress is generally the difference between the confining pressure and pore pressure. Scholars at home and abroad have carried out much research on the effect of effective stress on rock sonic velocity [20–27]. Wang et al. (2021) collected core samples from the Xiling mining area of the Sanshandao gold mine and conducted experimental analysis [28]. They believed that the vertical stress, maximum horizontal stress and minimum horizontal stress in the coastal mining area all increased in an approximate logarithmic function trend with increasing burial depth. The relationship between rock mechanical parameters and in situ stress is roughly logarithmic, and the influence of maximum horizontal stress on rock mechanical parameters is greater than that of minimum principal stress. Rock mechanical parameters have different effects on the value and direction of in situ stress.

Rock water saturation affects the sonic velocity [29]. Shi et al. (1995) studied sandstone in the Yulin area of Daqing Oilfield and found that shear wave velocity was constant with the change in water saturation [30]. When the water saturation was low, the velocity of the P-wave did not change with the change in saturation; when the water saturation was high, the velocity of the P-wave increased with increasing water saturation. Zhu et al. (2011) found that as the gas content of carbonate rocks increased, P-wave velocity decreased, while S-wave velocity changed little [31]. At present, experimental and numerical simulation methods are widely used to study the relationship between in situ stress and rock physical parameters [32–34]. Rock sonic velocity and resistivity are the key parameters of rock mechanics and reservoir physical properties. The study area of Tarim is in a strong stress environment. Strong stress will have a certain impact on porosity and acoustic velocity, causing effects that hamper a clear understanding of reservoir quality under the strong stress environment. This study combined the distribution of underground stress and designed an experimental scheme of in situ stress on rock physical parameters to explore the influence of stress anisotropy on rock physical parameters in deep and ultradeep tight sandstone.

2. Geological Setting

The Kuqa Depression, located at the junction of the Tarim Basin and Southern Tianshan Mountains, is a typical deep-ultradeep gas-rich area [35–37]. The Kelasu tectonic belt is the second row of the thrust belt in the northern Kuqa Depression, which was formed during the evolution of the Kuqa Depression. The burial depth is between 6000–8000 m, and it is an ultradeep reservoir. The Kelasu tectonic belt is divided into the Kela zone and Keshen zone, and the Keshen zone is divided into four sections from east to west, namely, Keshen, Dabei, Bozi and Awat (Figure 1). Ground stress and fracture development scale are important factors controlling production [38,39]. The Kuqa Depression experienced an evolution stage from a passive continental margin to a peripheral foreland basin in the late Permian to Triassic. Late Cretaceous regional uplift and denudation, regional peneplain stage; Paleogene weakly extensional tectonic setting; and Neogene to Quaternary compressive stress made the Kuqa Depression enter the evolutionary stage of the Paleozoic basin. The compression was most intense in the middle and late Neogene, and the current tectonic deformation of the Kelasu tectonic belt mainly occurred during this period [40]. The tectonic stress environment can be roughly divided into four periods. The Triassic compressional tectonic environment was mainly a contracting tectonic deformation. Based on stratigraphic and lithofacies data, the Kelasu tectonic belt through the Jurassic and Cretaceous periods was a variation zone with rapid thickening from south to north and had a regional tectonic setting with high-angle normal faults [41–43]. In the Paleogene, the relatively weak extensional tectonic stress environment or stable tectonic environment mainly formed depression basins and developed a large number of salt rocks. The Neogene to Quaternary compression in the near north–south region formed intercontinental or foreland-like basins before the new Tianshan intraplate orogenic belt [44].

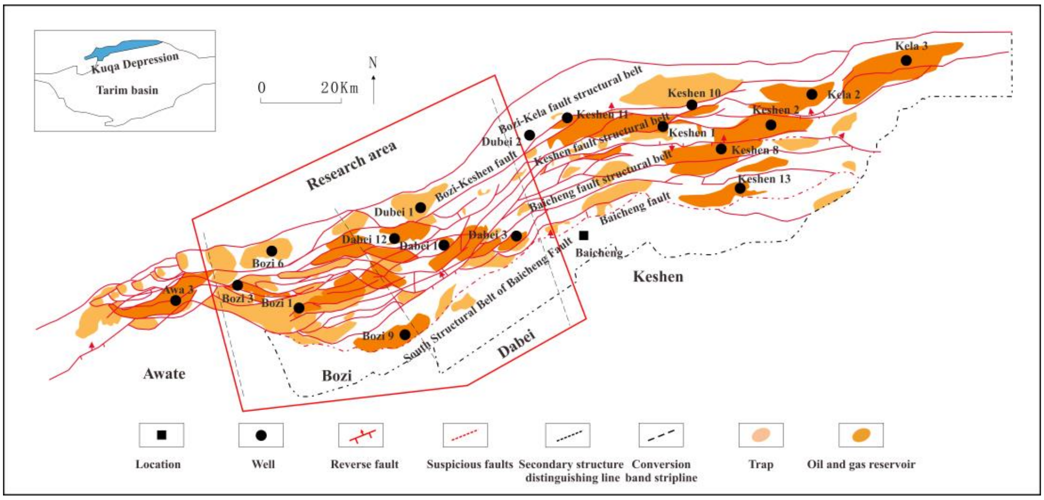

Figure 1. Fault Outline Map of Kelasu Structural Belt.

The strata of the Kelasu tectonic belt are divided into suprasalt strata, salt strata and subsalt strata. The subsalt strata include the Triassic, Jurassic and Lower Cretaceous strata. The salt rock is from the Paleogene Kumugeliemu Group. The upper and lower salt strata include the Suweiyi Group of Paleogene, Jidike Group of Neogene, Kangcun Group of Neogene, and Kuqa Group of the Neogene and Quaternary system [45–48]. In the late Cenozoic period, the Kuqa foreland thrust belt was strongly compressed. The anticlinal three-layer structure with different vertical stresses was formed by the tectonic compression of the southern Tianshan Mountains, the induction and equalization of the overlying salt layer, and the arch extension of the very thick mudstone of the Cretaceous Shushanhe

Group. Under the influence of stress, the Cretaceous Bashijiqike Group reservoir can be divided into a vertical three-layer structure, which consists of the stress sections of tensile, transitional, and compression torsion from top to bottom. In the longitudinal direction, the productivity of different stress sections varies greatly [49]. Zhang et al. (2004) used the fault slip data inversion method to recover Neogene paleotectonic stress in the Kuqa Depression based on field observations of faults developed in the Neogene, Paleogene and Cretaceous periods that were simultaneously involved in deformation [50]. The results show that the tectonic stress direction of the Kuqa Depression had little spatial variation in the Neogene and experienced a NNW–SSE compression deformation stage in the Miocene Jidike Group–Kangcun Group and a WNW–ESE compression deformation stage in the Pliocene Kuqa Group.

Reservoir heterogeneity is strong in the Kuqa Depression, which affects well productivity. In the depression, the productivity of gas wells with similar petrophysical properties in the same structure differs greatly, and even the productivity of two adjacent wells in the same structure differs significantly. Therefore, in situ stress-related factors should be considered in reservoir evaluation [51]. The gas reservoir is buried over more than 6500 m, which is a strike-slip stress field. Analysis of the numerical simulation results of the stress field shows that the present in situ stress is high, the horizontal stress difference is large, and the heterogeneity is strong. The maximum horizontal principal stress will be deflated in the plane and longitudinal directions, and the maximum deflection can be 90°. Complex geological boundary conditions and differences in rock mechanical properties are important factors for the strong heterogeneity of the in situ stress field distribution, and gas reservoir development affects the in situ stress state around wells [52].

The exploration breakthrough of Bozi 9 reflects the great difference in the structural transformation between different zones and the strong heterogeneity [39]. In the Kelasu tectonic belt, the reservoirs buried more than 4500 m are strike-slip fields in an in situ stress state. The maximum horizontal principal stress of the Dabei 12 gas reservoir is 125–161 MPa, the minimum horizontal principal stress is 118–130 MPa, and the maximum horizontal principal stress is always greater than the minimum horizontal principal stress. The heterogeneity of in situ stress is strong, and the difference between wells is large. The conditions of the complex geological boundary and the interbedded lithology of reservoirs result in an extremely heterogeneous distribution of in situ stress. Favorable and unfavorable areas of in situ stress are distributed alternately, and unfavorable areas of in situ stress may be encountered in high structural positions [51]. Zheng et al. (2016) recovered the Cenozoic tectonic stress field in the Kuqa Depression, and a study using elastic finite element numerical simulation showed that the direction of the maximum principal compressive stress in the Kuqa Depression in the late Himalayan period was generally nearly north–south, which was highly fitted with the paleostress field [53]. In the Yangxiahe area, the direction of the maximum principal stress is slightly deflected due to the influence of the turning point of the fold hub, which reflects the local stress direction.

3. Materials and Methods

3.1. Experimental Equipment and Experimental Samples

This experiment was mainly based on field samples to discuss the coupling relationship between stress and rock physical parameters. The experimental instrument used was an SCMS-SD, a high-temperature and high-pressure rock sonic electrical measuring instrument from China University of Petroleum (East China) (Figure 2). The experimental temperature was 24 °C. The P-wave frequency was 700 kHz, and the S-wave frequency was 400 kHz. The pore pressure was 0 MPa. Through experiments, the P-wave velocity, S-wave velocity and resistivity of each sample at different stress points were obtained.

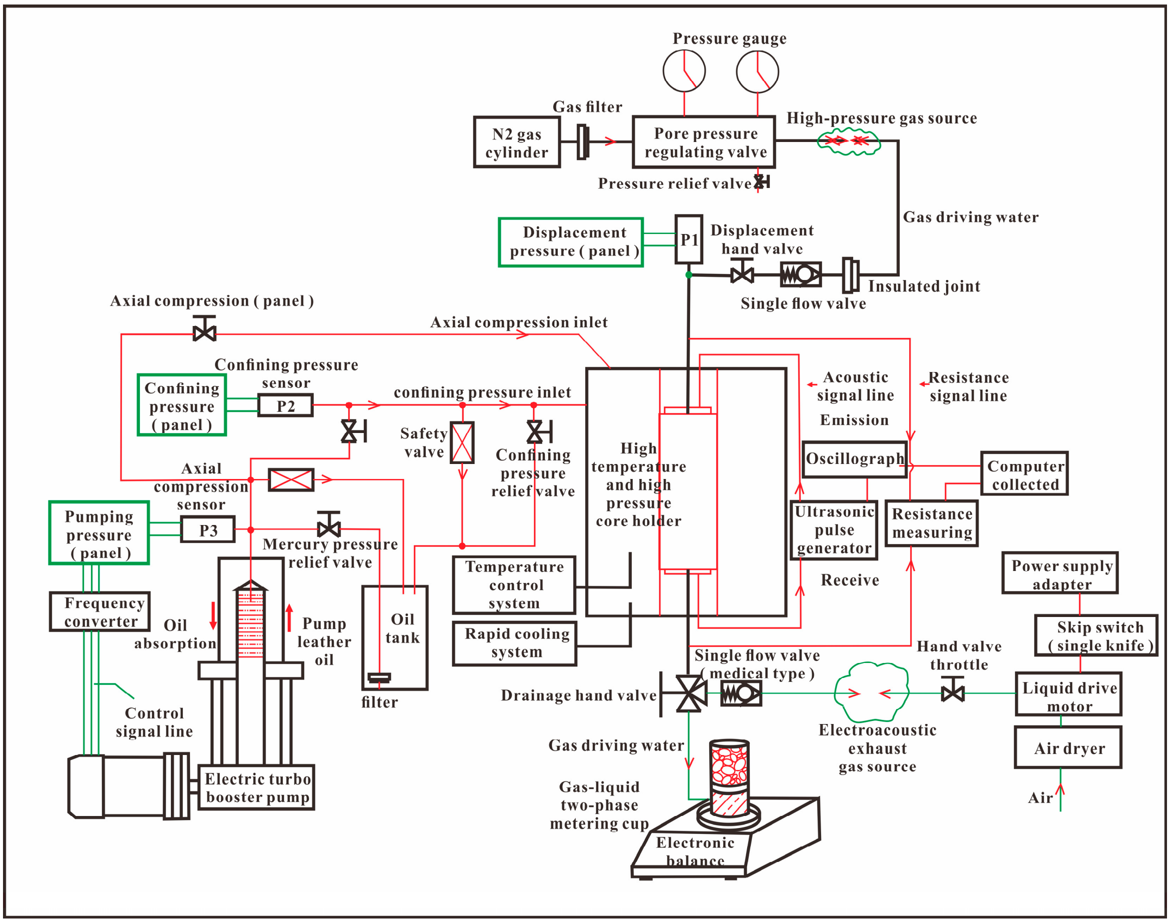

Figure 2. Working principle of the SCMS-SD, a high-temperature and high-pressure rock sonic electrical measuring instrument.

The experimental research area was the Kelasu tectonic belt in the Kuqa Depression, Tarim Basin. Samples were taken from field outcrops in the research area, and 22 experimental samples were evaluated. The samples were fine sandstone with an average sample size of 2.5 cm $\times$ 5.0 cm. A whole rock mineral experiment was conducted. The mineral composition of the field samples was similar to that of the core samples, and the material foundation of the field samples were good.

3.2. The Experimental Scheme

Since it is difficult to impose high pore pressure on tight sandstone, an effective stress scheme was used to analyze the effect of stress on rock physical parameters. Due to the scarcity of samples in this experiment, in order to consider the universality and accuracy of the experiment, the experimental scheme was set up according to the in situ formation conditions. According to the results of in situ stress logging interpretation (Figure 3), the in situ effective stress was determined, and the confining pressure and axial pressure were set. According to the experimental determination of in situ formation water salinity, the concentration of saturated brine was 150 g/L. The specific experimental scheme is shown in Table 1.

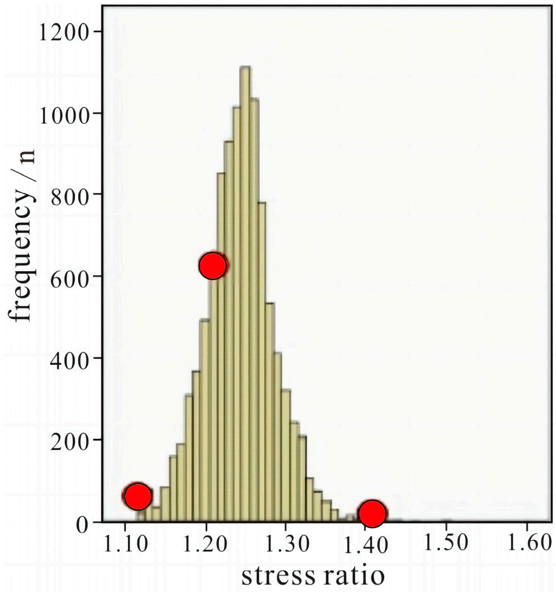

Figure 3. The stress ratio distribution frequency.

Table 1. The experimental scheme.

Analysis of the Factors	Clay Content/%	Water Saturation/%	Confining Pressure/MPa	Axial Pressure/MPa
Water saturation	24.2	0	60	78
	24.2	20	60	78
	24.2	40	60	78
	24.2	60	60	78
	24.2	80	60	78
	24.2	100	60	78
Horizontal maximum principal stress or horizontal minimum principal stress, buried depth	20.1	100	52	57.2
	20.1	100	56	67.2
	20.1	100	60	78
	20.1	100	64	89.6
Horizontal maximum principal stress or horizontal minimum principal stress, buried depth	16.9	100	44.6	58
	16.9	100	52.3	68
	16.9	100	60	78
	16.9	100	67.7	88
Confining pressure	13.7	100	50	78
	13.7	100	60	78
	13.7	100	70	78
	13.7	100	80	78
Axial pressure, stress ratio	8.4	100	60	66
	8.4	100	60	72
	8.4	100	60	78
	8.4	100	60	84

3.3. Experimental Equipment and Experimental Samples

To study the influence of water saturation on sonic and electrical parameters, the rock sample No. 3-11-8-1 was selected, and different water saturation levels for the experimental group were set as 0%, 50%, 64%, 78% and 100%. The confining pressure and axial pressure remained unchanged, at 60 MPa and 78 MPa, respectively (Figure 4). It is important to note that this experiment was repeated many times for the given samples to conduct the rock physical parameter tests under different conditions. The following experiments were the same, and there was no further elaboration.

Figure 4. The core before and after the experiment.

To study the influence of the stress ratio on the sonic and electrical parameters, the rock physical parameters of core No. 1-2-1 were tested. First of all, in this paper, the stress ratio, which is an important parameter reflecting the anisotropy of in situ stress, was defined as the ratio of axial pressure to confining pressure. Four experimental groups were set: (1) confining pressure of 52 MPa, axial pressure of 57.2 MPa, and stress ratio of 1.1; (2) confining pressure of 56 MPa, axial pressure of 67.2 MPa, and stress ratio of 1.2; (3) confining pressure of 60 MPa, axial pressure of 78 MPa, and stress ratio of 1.3; (4) confining pressure of 64 MPa, axial pressure of 89.6 MPa, and stress ratio of 1.4. The specific test scheme is shown in Table 2.

Table 2. The experimental scheme table.

Confining Pressure (MPa)	Axial Pressure (MPa)	Stress Ratio
52	57.2	1.1
56	67.2	1.2
60	78	1.3
64	89.6	1.4

To study the influence of the burial depth and confining pressure on the sonic and resistivity parameters, two types of experiments were set up. The specific experimental scheme is as follows:

(1) Rock physics experiments under the same stress ratio and different confining pressures

Four groups of rock physical parameters were tested for rock sample No. 1-2-2. The experimental conditions were as follows: (1) confining pressure of 44.6 MPa, axial pressure of 58 MPa, and stress ratio of 1.3; (2) confining pressure of 52.3 MPa, axial pressure of 68 MPa, and stress ratio of 1.3; (3) confining pressure of 60 MPa, axial pressure of 78 MPa, and stress ratio of 1.3; (4) confining pressure of 67.7 MPa, axial pressure of 88 MPa, and stress ratio of 1.3 (Table 3).

Table 3. 1-2-2 Sample experimental program.

Confining Pressure (MPa)	Axial Pressure (MPa)	Stress Ratio
44.6	58	1.3
52.3	68	1.3
60	78	1.3
67.7	88	1.3

To analyze the influence of the P-wave velocity, S-wave velocity, S-wave velocity ratio and resistivity on the confining pressure, the P-wave velocity, S-wave velocity ratio and resistivity were tested under confining pressures of 44.6 MPa, 52.3 MPa, 60 MPa and 67.7 MPa, respectively, and the stress ratio remained unchanged. The curves of P-wave velocity and confining pressure, S-wave velocity and confining pressure, P-S wave velocity ratio and confining pressure, and resistivity and confining pressure were fitted.

(2) Rock physics experiments under different confining pressures and different stress ratios

Rock physical parameters were tested for sample No. 3-2-14-1, which was divided into four experimental groups: (1) confining pressure of 50 MPa, axial pressure of 78 MPa, and stress ratio of 1.56; (2) confining pressure of 60 MPa, axial pressure of 78 MPa, and stress ratio of 1.30; (3) confining pressure of 70 MPa, axial pressure of 78 MPa, and stress ratio of 1.11; and (4) confining pressure of 80 MPa, axial pressure of 78 MPa, and stress ratio of 0.975 (Table 4).

Table 4. The experimental scheme for sample No. 3-2-14-1.

Confining Pressure (MPa)	Axial Pressure (MPa)	Stress Ratio
50	78	1.56
60	78	1.30
70	78	1.11
80	78	0.975

To analyze the relationship between the P-S wave velocity ratio, resistivity and confining pressure, the P-S wave velocity ratio and resistivity output of rock samples under the same coaxial pressure and different confining pressures were recorded, and the curves of the relationship between the P-S wave velocity ratio, resistivity and confining pressure were fitted.

When studying the influence of axial compression on sonic and resistivity, the rock physical parameters of sample No. 3-10-5-1 were divided into four experimental groups for testing: (1) confining pressure of 60 MPa, axial pressure of 66 MPa, and stress ratio of 1.1; (2) confining pressure of 60 MPa, axial pressure of 72 MPa, and stress ratio of 1.2; (3) confining pressure of 60 MPa, axial pressure of 78 MPa, and stress ratio of 1.3; (4) confining pressure of 60 MPa, axial pressure of 84 MPa, and stress ratio of 1.4 (Table 5).

Table 5. The experimental scheme for sample No. 3-10-5-1.

Confining Pressure (MPa)	Axial Pressure (MPa)	Stress Ratio
60	66	1.1
60	72	1.2
60	78	1.3
60	84	1.4

Axial pressure affects the velocity ratio and resistivity of the S-waves and P-waves. When the confining pressure was constant, the velocity ratio and resistivity of the S-wave and P-wave output of the rock samples under different axial pressures were tested, and the relationships between the S-wave and P-wave velocity ratio, resistivity and axial pressure were drawn.

4. Results and Discussion

4.1. Influence of Water Saturation on Sonic and Electrical Parameters

Rock sample No. 3-11-8-1 was tested, and the P-wave signal change waveform and S-wave signal change waveform of different water saturations were output (Figure 5a,b).

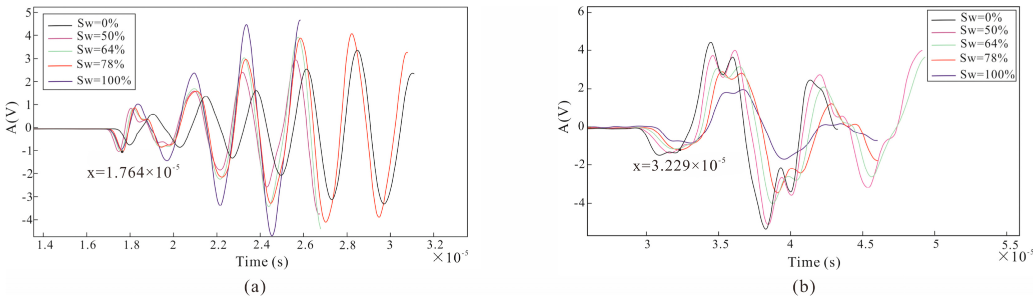

Figure 5. Waveform diagrams of P-wave (**a**) and S-wave (**b**) signal variation.

Rock water saturation affects the size of rock physical parameters. The P-wave velocity, S-wave velocity and resistivity of rock samples with water saturations of 0%, 50%, 64%, 78%, and 100% were statistically analyzed and fitted to the curves. The experimental results show that (1) with increasing water saturation, the P-wave velocity changed in three stages. When the water saturation was 0–23%, the P-wave velocity increased with increasing water saturation, and the slope was large. When the water saturation was 23–78%, the P-wave velocity decreased with increasing water saturation. When the water saturation was between 78% and 100%, the P-wave velocity decreased with increasing water saturation (Figure 6a). (2) The S-wave velocity decreased linearly with increasing water saturation, and there was a negative correlation between the S-wave velocity and water saturation (Figure 6b). (3) When the water saturation was less than 70%, the resistivity decreased with increasing water saturation. When the water saturation was greater than 70%, the resistivity was basically unchanged with increasing water saturation (Figure 6c). In general, with the change in water saturation, the shear modulus will change, which will lead to changes in longitudinal and transverse wave velocity.

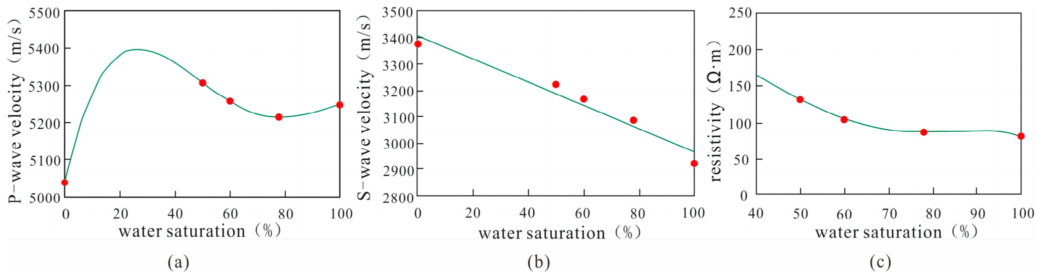

Figure 6. Relationship curves between P-wave velocity, S-wave velocity, resistivity and water saturation.

The mineral composition of rock affects the scale of rock physical parameters. In the experiment, rock samples with different contents of feldspar, quartz and clay were set up to output the velocity ratio of each rock sample. The points of different feldspar contents and their corresponding ratios, different quartz contents and their corresponding ratios, and different clay contents and their corresponding ratios were cast and fitted to the curves. The experimental results show that (1) there was an approximately positive correlation between the velocity ratio of the P-S wave and feldspar content (Figure 7a), and (2) there was a positive correlation between the P-S wave velocity ratio and quartz content (Figure 7b). (3) The ratio of the P-S wave velocity was positively correlated with the clay content (Figure 7c). (4) The rocks in the study area are mainly quartz minerals. Quartz plays a major role in the influence of P-wave and S-wave velocity, followed by feldspar and clay.

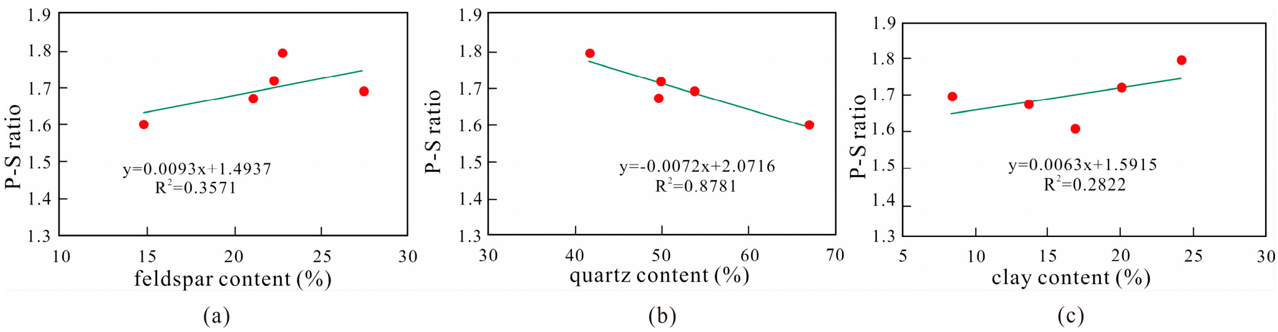

Figure 7. Relationship curves between feldspar content, quartz content, clay content and aspect ratio.

4.2. Influence of the Stress Ratio on the Sonic and Electrical Parameters

(1) The relationship between the resistivity and stress ratio

To analyze the resistivity affected by the stress ratio, the resistivity of the four experimental groups was tested, and the fitting curve was fitted with the stress ratio as the abscissa and resistivity as the ordinate. The experimental results show that the resistivity increased linearly with increasing stress ratio. The resistivity was positively correlated with the stress ratio (Figure 8).

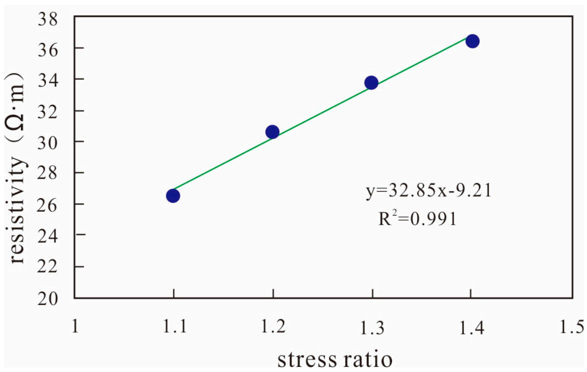

Figure 8. Relationship curve between resistivity and stress ratio.

(2) The relationship between the P-wave velocity, S-wave velocity, S-wave velocity ratio and stress ratio

The four experimental groups were set up to test the P-wave velocity, S-wave velocity and S-wave velocity ratio corresponding to different stress ratios, and fitting curves of P-wave velocity, S-wave velocity, S-wave velocity ratio and stress ratio were generated. The results show that (1) the P-wave velocity increased with increasing stress ratio (Figure 9a) and (2) the S-wave velocity was consistent with the P-wave velocity and positively correlated with the stress ratio, which was significantly smaller (Figure 9b). (3) There was a negative correlation between the stress ratio and S-wave ratio (Figure 9c).

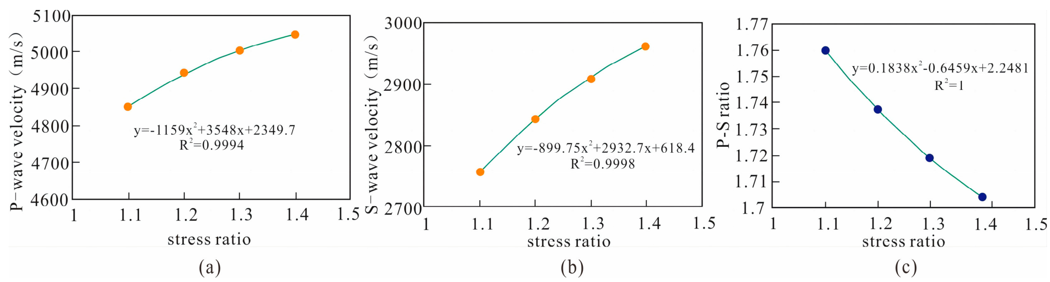

Figure 9. Relationship curves between the P-wave velocity, S-wave velocity, S-wave ratio and stress ratio.

4.3. Influence of Burial Depth and Confining Pressure on Sonic and Resistivity Parameters

(1) Rock physics experiments under the same stress ratio and different confining pressures

Four groups of rock physical parameters were tested for rock sample No. 1-2-2, and the results show that (1) the P-wave velocity increased logarithmically with increasing confining pressure (Figure 10a) and (2) the S-wave velocity, similar to the P-wave velocity, had a positive logarithmic correlation with confining pressure. The S-wave velocity changed with the confining pressure in a slightly larger amplitude than the P-wave velocity (Figure 10b). (3) The P-S wave velocity ratio was negatively correlated with the confining pressure and decreased logarithmically with increasing confining pressure (Figure 11a). (4) There was a positive correlation between resistivity and confining pressure (Figure 11b).

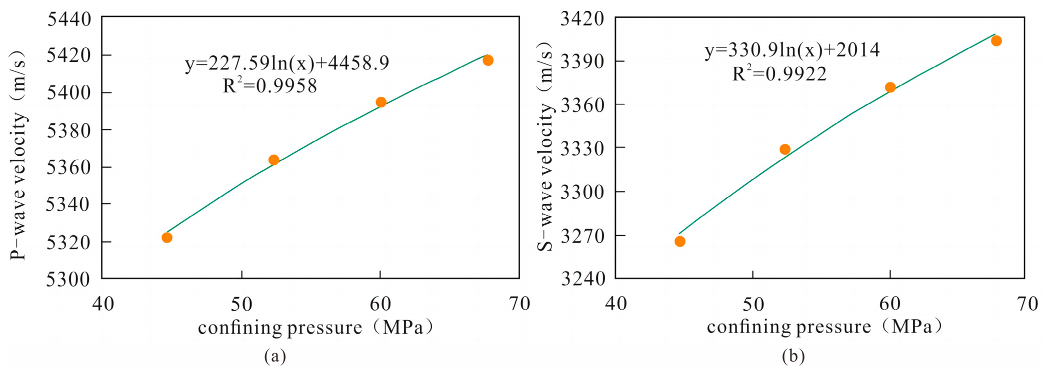

Figure 10. Curves of P-wave velocity, S-wave velocity and confining pressure.

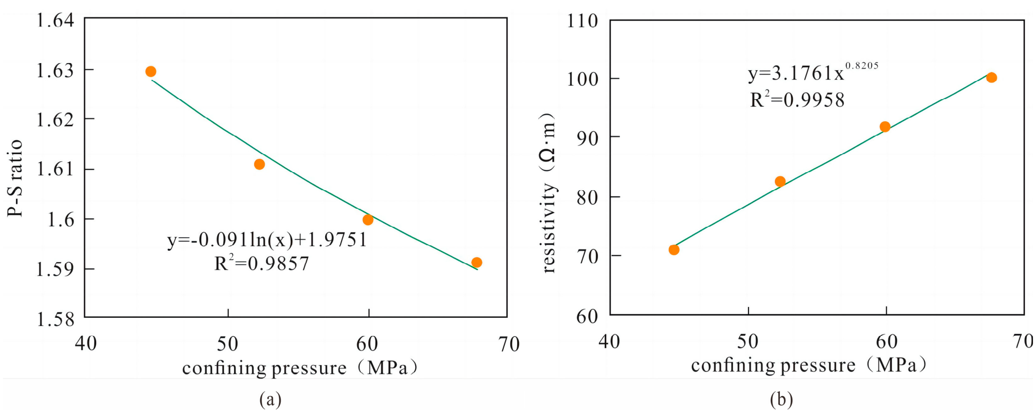

Figure 11. Curves of P-S wave ratio, resistivity and confining pressure.

(2) Rock physics experiments under different confining pressures

Four groups of rock physical parameters were tested for rock sample No. 3-2-14-1, and the results show that the P-S wave velocity ratio decreased with increasing confining pressure (Figure 12a). The resistivity increased with increasing confining pressure (Figure 12b).

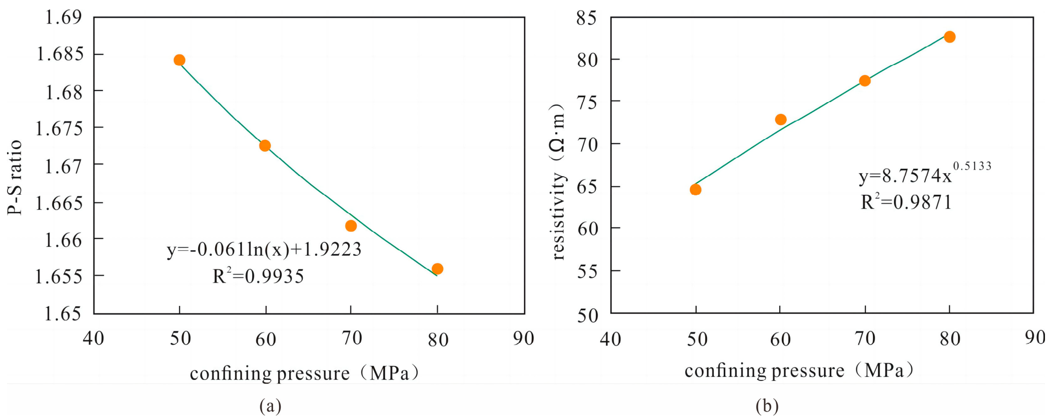

Figure 12. Relationship curves between P-S wave ratio, resistivity and confining pressure.

4.4. Influence of Axial Compression on Sonic Velocity and Resistivity

Four groups of rock physical parameters were tested for rock sample No. 3-10-5-1, and the results show that (1) the S-wave and P-wave ratios varied with axial compression in two stages. When the axial pressure was less than 80 MPa, the P-S wave velocity ratio decreased with increasing axial pressure. When the axial pressure was greater than 80 MPa, the P-S wave velocity ratio increased with increasing axial pressure (Figure 13a). (2) The resistivity increased with increasing axial pressure (Figure 13b).

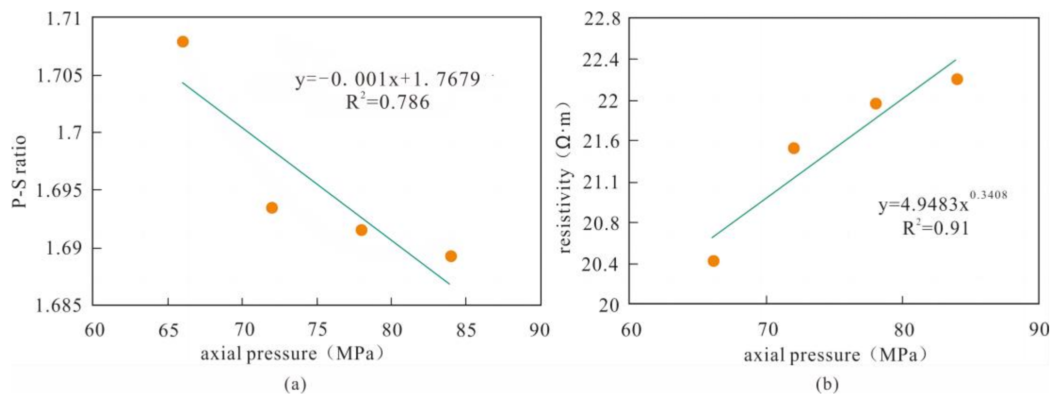

Figure 13. Correlation curves between P-S wave ratio, resistivity and axial pressure.

5. Conclusions

(1) Rock sonic velocity is extremely sensitive to water saturation under overburden pressure. At ultrasonic frequencies, when the water saturation increases from 0% to 80%, the P-wave velocity increased first and then decreased. When the water saturation continued to increase to 100%, the P-wave velocity increased. Saturation was negatively correlated with S-wave velocity and resistivity. This is because the shear modulus will change with the change in water saturation, which will lead to changes in longitudinal and transverse wave velocity.

(2) Different minerals have different controlling effects on the velocity ratio of S-waves and P-waves in rocks, and quartz content plays the main controlling role, which was negatively correlated with the ratio, followed by feldspar and clay, which were positively correlated with the ratio.

(3) The confining pressure, axial pressure, stress ratio and burial depth were positively correlated with the P-S wave but negatively correlated with the P-S wave ratio. The order of influencing factors were the stress ratio > confining pressure > axial pressure.

(4) In general, the experiment demonstrated the influence mechanism of strong stress on reservoir quality in the Tarim study area, but the experiment was not perfect. The rock surrounding the experiment site was not under true triaxial confining pressure. We

simulated the condition of biaxial compression, not true triaxial confining pressure. At the same time, the influence of underground pore pressure was less considered, so as a next step, we will consider the influence of true triaxial compression and underground pore pressure.

Author Contributions: Conceptualization, H.Z.; Funding acquisition, H.Z.; Investigation, G.Y.; Methodology, H.Z., K.X., B.Z. and C.L.; Project administration, H.Z.; Software, K.X., B.Z., H.W., S.L. and Z.Q.; Validation, Z.W., S.L. and Z.Q.; Visualization, H.W. and S.L.; Writing—original draft, H.Z., K.X., B.Z., G.Y., H.W., Z.W. and C.L. All authors have read and agreed to the published version of the manuscript.

Funding: This study was funded by the Major National Science and Technology Project (2016ZX05051), Major Science and Technology Project of PetroChina Company (2018E-1803).

Institutional Review Board Statement: Not applicable.

Informed Consent Statement: Not applicable.

Data Availability Statement: Not applicable.

Conflicts of Interest: H.Z., K.X., G.Y., H.W., Z.W., C.L., S.L. and Z.Q. were employed by Tarim Oilfield Company, PetroChina. The remaining author declares that the research was conducted in the absence of any commercial or financial relationships that could be construed as a potential conflict of interest.

References

1. Li, H.; Tang, H.; Qin, Q.; Zhou, J.; Qin, Z.; Fan, C.; Su, P.; Wang, Q.; Zhong, C. Characteristics, formation periods and genetic mechanisms of tectonic fractures in the tight gas sandstones reservoir: A case study of Xujiahe Formation in YB area, Sichuan Basin, China. *J. Pet. Sci. Eng.* **2019**, *178*, 723–735. [CrossRef]
2. Li, J.; Li, H.; Yang, C.; Wu, Y.; Gao, Z.; Jiang, S. Geological Characteristics and Controlling Factors of Deep Shale Gas Enrichment of the Wufeng-Longmaxi Formation in the Southern Sichuan Basin, China. *Lithosphere* **2022**, *2022*, 4737801. [CrossRef]
3. Zhang, H.; Xu, G.; Zhan, H.; Li, X.; He, J. Simulation of multi-period paleotectonic stress fields and distribution prediction of natural Ordovician fractures in the Huainan coalfield, Northern China. *J. Hydrol.* **2022**, *612*, 128291. [CrossRef]
4. Almqvist, B.S.; Hirt, A.M.; Herwegh, M.; Ebert, A.; Walter, J.M.; Leiss, B.; Burlini, L. Seismic anisotropy in the Morcles nappe shear zone: Implications for seismic imaging of crustal scale shear zones. *Tectonophysics* **2013**, *603*, 162–178. [CrossRef]
5. Bezrodna, I.; Bezrodnyi, D.; Kozionova, O. Analysis of impact of mineral matrix of runovshchinska area reservoir rocks on the elastic and acoustic parameters (based on the results of mathematical modelling). *Visnyk Taras Shevchenko Natl. Univ. Kyiv. Geol.* **2017**, *2*, 52–58. [CrossRef]
6. De Jonge-Anderson, I.; Ma, J.; Wu, X.; Stow, D. Determining reservoir intervals in the Bowland Shale using petrophysics and rock physics models. *Geophys. J. Int.* **2022**, *228*, 39–65. [CrossRef]
7. Dewangan, S.; Chattopadhyaya, S. Characterization of Wear Mechanisms in Distorted Conical Picks After Coal Cutting. *Rock Mech. Rock Eng.* **2016**, *49*, 225–242. [CrossRef]
8. Dewangan, S.; Chattopadhyaya, S.; Hloch, S. Wear Assessment of Conical Pick used in Coal Cutting Operation. *Rock Mech. Rock Eng.* **2015**, *48*, 2129–2139. [CrossRef]
9. Eberhart-Phillips, D.; Han, D.-H.; Zoback, M.D. Empirical relationships among seismic velocity, effective pressure, porosity, and clay content in sandstone. *Geophysics* **1989**, *54*, 82–89. [CrossRef]
10. Faccenda, M.; Bressan, G.; Burlini, L. Seismic properties of the upper crust in the central Friuli area (northeastern Italy) based on petrophysical data. *Tectonophysics* **2007**, *445*, 210–226. [CrossRef]
11. Liu, J.; Ding, W.; Yang, H.; Wang, R.; Yin, S.; Li, A.; Fu, F. 3D geomechanical modeling and numerical simulation of in-situ stress fields in shale reservoirs: A case study of the lower Cambrian Niutitang formation in the Cen'gong block, South China. *Tectonophysics* **2017**, *712–713*, 663–683. [CrossRef]
12. Liu, J.; Mei, L.; Ding, W.; Xu, K.; Yang, H.; Haimeng, Y. Asymmetric propagation mechanism of hydraulic fracture networks in continental reservoirs. *GSA Bull.* **2022**. [CrossRef]
13. Wyllie, M.R.J.; Gregory, A.R.; Gardner, G.H.F. An experimental investigation of factors affecting elastic wave velocities in porous media. *Geophysics* **1958**, *23*, 459–493. [CrossRef]
14. Birch, F. Elastic constants of rutile-A correction to a paper by R. K. Verma, "Elasticity of some high-density crystals". *J. Geophys. Res. Earth Surf.* **1960**, *65*, 3855–3856. [CrossRef]
15. Han, D.; Nur, A.; Morgan, D. Effects of porosity and clay content on wave velocities in sandstones. *Geophysics* **1986**, *51*, 2093–2107. [CrossRef]
16. Tutuncu, A.N.; Podio, A.L.; Sharma, M.M. An experimental investigation of factors influencing compressional- and shear-wave velocities and attenuations in tight gas sandstones. *Geophysics* **1994**, *59*, 77–86. [CrossRef]

17. Ma, Z.G.; Wu, X.Y.; Wang, Z.H. Effect of effective pressure on compressional and shear wave velocities. *Prog. Explor. Geophys.* **2006**, *29*, 183–186. (In Chinese)
18. Xiao, W.L.; Li, M.; Zhao, J.Z.; Zheng, L.L.; Li, L.J. Laboratory study of stress sensitivity to permeability in tight sandstone. *Rock Soil Mech.* **2010**, *31*, 775–779. [CrossRef]
19. Wang, K.; Dai, J.S.; Zhang, H.G.; Zhang, D.D.; Zhao, L.B. Numerical simulation of fractured reservoir stress sensi-tivity: A case from Kuqa depression Keshen gas field. *Acta Pet. Sin.* **2014**, *35*, 123. [CrossRef]
20. Ali, M. "Double Peak" of Dynamic Strengths and Acoustic Emission Responses of Coal Masses Under Dynamic Loading. *Nonrenewable Resour.* **2022**, *31*, 1705–1720. [CrossRef]
21. Jia, D.; Qiu, Y.; Li, C.; Cai, Y. Propagation of pressure drop in coalbed methane reservoir during drainage stage. *Adv. Geo-Energy Res.* **2019**, *3*, 387–395. [CrossRef]
22. Lv, A.; Aghighi, M.A.; Masoumi, H.; Roshan, H. The effects of sorbing and non-sorbing gases on ultrasonic wave propagation in fractured coal. *Int. J. Coal Geol.* **2022**, *249*, 103906. [CrossRef]
23. Moarefvand, A.; Gasc, J.; Fauconnier, J.; Baïsset, M.; Burdette, E.; Labrousse, L.; Schubnel, A. A new generation Griggs apparatus with active acoustic monitoring. *Tectonophysics* **2021**, *816*, 229032. [CrossRef]
24. Sethi, H.; Shragge, J.; Tsvankin, I. Tensorial elastodynamics for coupled acoustic/elastic anisotropic media: Incorporating bathymetry. *Geophys. J. Int.* **2022**, *228*, 999–1014. [CrossRef]
25. Shen, H.; Li, X.; Li, Q. Influence of the microstructure on stress-dependent *P*-wave anisotropy in sandstone. *Geophys. J. Int.* **2022**, *228*, 876–892. [CrossRef]
26. Traylor, T.K.; Burnley, P.C.; Whitaker, M.L. Initial Acoustoelastic Measurements in Olivine: Investigating the Effect of Stress on *P*- and *S*-Wave Velocities. *J. Geophys. Res. Solid Earth* **2021**, *126*, e2021JB022494. [CrossRef]
27. Zhang, X.B.; Wang, X.T.; Liu, B.H.; Song, P.; Tan, J.; Xie, C. Reverse time migration based on the pseudo-space-domain first-order velocity-stress acoustic wave equation. *Front. Earth Sci.* **2021**, *9*, 690513. [CrossRef]
28. Wang, X.; Ma, C.D.; Liu, X.Q.; Jiang, M.W.; Fan, Y.Y. The Variation Law of In-situ Stress and Rock Mechanical Parameters with Buried Depth in Coastal Mining Area and Their Relationship. *Gold Sci. Technol.* **2021**, *29*, 535–544. [CrossRef]
29. Douma, L.A.N.R.; Dautriat, J.; Sarout, J.; Dewhurst, D.N.; Barnhoorn, A. Impact of water saturation on the elastic anisotropy of the Whitby Mudstone, United Kingdom. *Geophysics* **2020**, *85*, MR57–MR72. [CrossRef]
30. Shi, X.J.; Xu, H.M.; Xie, D.; Xu, G.M.; Wang, Y.Z.; Wei, J.X. Wave velocity in reservoir-conditioned rock and its variation. *OGP* **1995**, *30*, 386–391. (In Chinese)
31. Zhu, H.L.; Liu, X.J.; Liu, H. Experimental research on effects of gas saturation on acoustic wave velocity of carbonate rock. *Chin. J. Rock Mech. Eng.* **2011**, *30*, 2784–2789.
32. Cai, J.; Zhao, L.; Zhang, F.; Wei, W. Advances in multiscale rock physics for unconventional reservoirs. *Adv. Geo-Energy Res.* **2022**, *6*, 271–275. [CrossRef]
33. Chen, X.; Zhou, Y. Applications of digital core analysis and hydraulic flow units in petrophysical characterization. *Adv. Geo-Energy Res.* **2017**, *1*, 18–30. [CrossRef]
34. Liu, J.S.; Ding, W.L.; Yang, H.M.; Dai, P.; Wu, Z.H.; Zhang, G.J. Natural Fractures and Rock Mechanical Stratigraphy Evaluation in the Huaqing area, Ordos Basin: A Quantitative Analysis Based on Numerical Simulation. *J. China Univ. Geosci.* **2022**, 1–19. Available online: http://kns.cnki.net/kcms/detail/42.1874.P.20220711.0942.004.html (accessed on 21 September 2022).
35. Fan, C.; Wang, G.; Wang, Z.; Han, X.; Chen, J.; Zhang, K.; Zhang, B. Prediction of multiple origin overpressure in deep fold-thrust belt: A case study of Kuqa subbasin, Tarim Basin, northwestern China. *AAPG Bull.* **2021**, *105*, 1511–1533. [CrossRef]
36. Gao, Z.Y.; Feng, J.R.; Cui, J.G.; Wang, X.Q.; Zhou, C.M.; Shi, Y.X. Physical simulation and quantitative calculation of increased feldspar dissolution pores in deep reservoirs. *Pet. Explor. Dev.* **2017**, *44*, 387–398. [CrossRef]
37. Guo, X.; Liu, K.; Jia, C.; Song, Y.; Zhao, M.; Zhuo, Q.; Lu, X. Effects of tectonic compression on petroleum accumulation in the Kelasu Thrust Belt of the Kuqa Sub-basin, Tarim Basin, NW China. *Org. Geochem.* **2016**, *101*, 22–37. [CrossRef]
38. Tang, Y.G.; Zhou, P.; Xu., Z.P.; Yin, H.W.; Zhu, W.H.; Xie, Y.N. The influence of stress environment on reservoir under salt in Kelasu structure belt. *Geol. J. China Univ.* **2017**, *23*, 95–103. [CrossRef]
39. Wei, G.Q.; Wang, J.P.; Zeng, L.B.; Tang, Y.L.; Wang, K.; Liu, T.T.; Yang, Y. Structural reworking effects and new exploration discoveries of subsalt ultra-deep reservoirs in the Kelasu tectonic zone. *Nat. Gas Ind.* **2020**, *40*, 20–30.
40. Yang, K.J.; Qi, J.F.; Ma, B.J.; Sun, T.; Zhang, X.C.; Zhang, S. Differential tectonic deformation of subsalt and supras-alt strata in Kuqa Depression and their controlling factors. *Geotecton. Metallog.* **2018**, *42*, 211–224. [CrossRef]
41. Sun, S.; Hou, G.; Zheng, C. Fracture zones constrained by neutral surfaces in a fault-related fold: Insights from the Kelasu tectonic zone, Kuqa Depression. *J. Struct. Geol.* **2017**, *104*, 112–124. [CrossRef]
42. Tian, Z.; Sun, J.; Windley, B.F.; Zhang, Z.; Gong, Z.; Lin, X.; Xiao, W. Cenozoic detachment folding in the southern Tianshan foreland, NW China: Shortening distances and rates. *J. Struct. Geol.* **2016**, *84*, 142–161. [CrossRef]
43. Wang, W.; Yin, H.; Jia, D.; Li, C. A sub-salt structural model of the Kelasu structure in the Kuqa foreland basin, northwest China. *Mar. Pet. Geol.* **2017**, *88*, 115–126. [CrossRef]
44. Guo, W.X.; Qi, J.F.; Li, M.G.; Lei, G.L.I.; Li, Y.Y. Inversion structure of Kelasu structure zone in Kuqa depression and its formation mechanism. *Acta Pet. Sin.* **2010**, *31*, 379–385. [CrossRef]
45. Li, S.; Li, F.; Qiu, Y.; Yan, Y. A numerical study on the regional in situ stress field of the Keshen section and interface dislocation in the composite salt-gypsum layer. *Interpretation* **2020**, *8*, T803–T811. [CrossRef]

46. Lyu, C.; Wang, X.; Lu, X.; Zhou, Q.; Zhang, Y.; Sun, Z.; Xiao, L.; Liu, X. Evaluation of Hydrocarbon Generation Using Structural and Thermal Modeling in the Thrust Belt of Kuqa Foreland Basin, NW China. *Geofluids* **2020**, *2020*, 8894030. [CrossRef]
47. Nian, T.; Wang, G.; Xiao, C.; Zhou, L.; Sun, Y.; Song, H. Determination of in-situ stress orientation and subsurface fracture analysis from image-core integration: An example from ultra-deep tight sandstone (BSJQK Formation) in the Kelasu Belt, Tarim Basin. *J. Pet. Sci. Eng.* **2016**, *147*, 495–503. [CrossRef]
48. Song, X.; Lü, X.; Shen, Y.; Guo, S. Hydrocarbon migration and accumulation history in deep reservoirs: A case study of Mesozoic sandstone gas reservoirs in the Kelasu-Yiqikelike structural belt of the Kuqa Depression, Tarim Basin. *Geosci. J.* **2019**, *23*, 69–86. [CrossRef]
49. Shi, L.L.; Tang, Y.Y.; Wang, B.; Wang, Z.T.; Wei, H.X.; Zhou, L. Characteristics of Vertical Zonation of Bashijiqike Reservoir by Stress Intervals in Wellblock Keshen5 in Kuqa Depression, Tarim Basin. *Xinjiang Pet. Geol.* **2016**, *37*, 1. [CrossRef]
50. Zhang, Z.P.; Wang, Q.C. The summary and comment on fault-slip analysis and palaeostress reconstruction. *Adv. Earth Sci.* **2004**, *19*, 605–613.
51. Xu, K.; Zhang, H.; Liu, X.Y.; Wang, Z.M.; Lai, S.J. Current in-situ stress characteristics of deep fractured reservoirs in Kuqa Depression and its guiding significance to natural gas exploration and development. *Editor. Dep. Pet. Geol. Recovery Effic.* **2022**, *29*, 34–45. [CrossRef]
52. Xu, K.; Yang, H.J.; Zhang, H.; Wang, H.Y.; Yuan, F.; Wang, H.H.; Li, C. Current In-Situ Stress Field and Efficient Development of Bozi-1 Gas Reservoir in Kelasu Structural Belt. *Xinjiang Pet. Geol.* **2021**, *42*, 726–734.
53. Zheng, C.F.; Hou, G.T.; Zhan, Y.; Yu, X.; Zhao, W.T. An analysis of Cenozoic tectonic stress fields in the Kuqa depression. *Geol. Bull. China* **2016**, *35*, 130–139.